Ultra-precision Machining of Hard and Brittle Materials with Coarse-Grained Grinding Wheels

Bing Guo and Qingliang Zhao

Abstract Many attempts have been made to achieve optical surfaces on hard and brittle materials by means of ductile diamond grinding using fine-grained diamond wheels. However, the large wear rate of the fine-grained grinding wheel, which is caused by dressing and by the grinding process, limited the achievable form accuracy and the maximum material removal volume, especially in case of ductile grinding of large optical surfaces. For solving this problem, a novel-type diamond wheel must be applied which features much higher grinding ratios than that of fine-grained diamond wheels to guarantee the machined surface form accuracy in ultra-precision grinding of hard and brittle materials. In this chapter, the precision conditioning methods of coarse-grained diamond wheels for ultra-precision grinding will be presented first. Subsequently, the ultra-precision grinding of hard and brittle materials with coarse-grained grinding wheels will be investigated in order to reveal the performance of these novel diamond wheels. To conclude the chapter, micro-structured surface will be machined on the diamond grain surfaces of coarse-grained wheels for improving ground subsurface damage.

1 Introduction

Ultra-precision grinding of hard and brittle materials such as optical glass, ceramics, cemented carbides, and crystal materials has been applied in a wide range of applications in order to obtain high-quality surfaces with nanoscale roughness, submicron form accuracy, and micron-level subsurface damage. Commonly, fine-grained grinding wheels with diamond grain diameter from several micrometers down to sub-micrometer are mainly used for ultra-precision grinding various hard and brittle materials [1]. According to many research results, the smaller the abrasive grain size, the better the final finished surface roughness and integrity [2–4]. However, the high

B. Guo (✉) · Q. Zhao
Center for Precision Engineering, School of Mechatronics Engineering,
Harbin Institute of Technology, Harbin 150001, China
e-mail: guobing@hit.edu.cn

wear rate and self-sharpening effects of the wheel bonding system, wheel loading as well as periodic conditioning requirement of fine-grained grinding wheels deteriorate the form accuracy of the machined surface and simultaneously introduce a lower grinding efficiency [5–7].

For solving these problems, a novel diamond wheel must be applied which features much higher grinding ratios to guarantee the form accuracy in ultra-precision grinding of hard and brittle materials. The applied wheels should have the following characteristics:

1. Bigger grain size than fine-grained wheels for resisting abrasive wear;
2. Higher bonding strength to avoid the loss of abrasives;
3. Required constant wheel peripheral envelope surface for ensuring homogeneous undeformed chip thickness.

Monolayer coarse-grained diamond grinding wheel featuring grain sizes of more than 100 μm fulfills most of the above-mentioned requirements. Therefore, it could be a solution for the wheel wear problem incurred by fine-grained diamond wheels, provided that they are well conditioned in terms of minimized wheel run-out error, constant wheel peripheral envelope, as well as top-flattened diamond grains with required grain protrusion height of at least a few micrometers.

Generally, monolayer coarse-grained diamond wheel is not usually conditioned in the grinding process. On the one hand, they are mainly applied in rough grinding, which means the wheel conditioning is unnecessary. On the other hand, monolayer coarse-grained diamond wheels only have a single abrasive layer which easily led to damage of the abrasive layer before the conditioning of diamond grains themselves [8]. However, nowadays improved manufacturing technique can make the monolayer diamond wheel superior in terms of wheel's higher geometrical accuracy (base run-out and homogenous deposited bonding layer depth), the bigger bonding strength between base surface and bonding layer, as well as the holding strength of the grains inside bonding layer. Besides, if the on-site conditioning of monolayer coarse-grained diamond wheels could be precisely controlled, the coarse-grained diamond wheels will have a constant wheel peripheral envelope surface, then the ultra-precision grinding of hard and brittle materials could be realized.

2 On-site Precise Conditioning of Coarse-Grained Grinding Wheels

For conventional coarse-grained diamond wheels, the diamond grains with different protrusion heights and the wheel manufacturing deviation will result in a different depth of grinding. In grinding process, some diamond grains will penetrate beyond the critical depth of cut and induce brittle damage, as shown in Fig. 1. Hence, in order to realize the ultra-precision grinding of hard and brittle materials with coarse-grained diamond wheels, an efficient conditioning technique must be developed to guarantee diamond grains with a constant wheel peripheral envelope surface. To meet
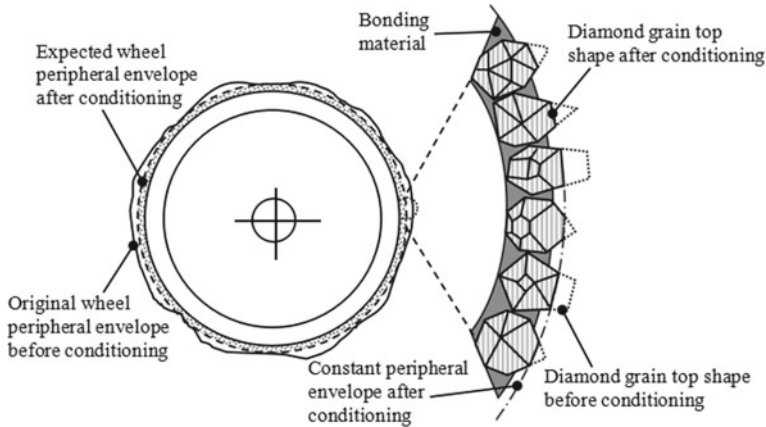
Fig. 1 Sketch map of coarse-grained diamond wheels for ultra-precision grinding of hard and brittle materials

this requirement, three kinds of on-site conditioning technique were adopted for conditioning the coarse-grained diamond wheels including electrolytic in-process dressing (ELID)-assisted conditioning with metal bond diamond truer, thermochemical conditioning with metal truer, and mechanical conditioning with vitrified diamond truer.

2.1 ELID-Assisted Conditioning of Coarse-Grained Grinding Wheels

Dressing of grinding wheels based on the oxidation of the metal bond was initially developed by Ohmori and Nakagawa [9]. Here, the ELID technique was used for the metal bond diamond truer in order to avoid the loading, leading to a continuous and stable conditioning process. Unlike the fine-grained diamond wheel, in this conditioning process, not the bond material but the outstanding tops of diamond grits were cut off in order to insure the diamond grains within a constant wheel peripheral envelope surface.

An experimental system illustrated in Fig. 2 was developed. The metal bond diamond truer with 91-μm grain size was mounted on the work spindle which was dressed in-process by ELID method. The interaction between the grinding wheel and the truer was a truncating mechanism along with the motion in X- and Z-directions, eventually resulting in flattened grains, until finally a constant grain peripheral envelope was obtained. The parameters of 60 V, 40% duty, and 20 A current were used for ELID system. The D151 monolayer nickel electroplated diamond wheels were adopted. The conditioning parameters were grinding wheel speed of 5000 rpm, infeed
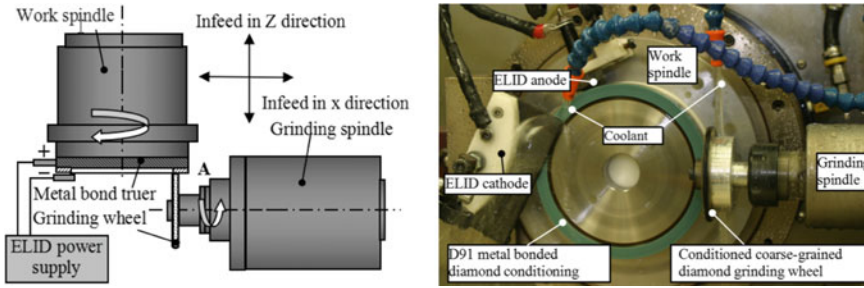
Fig. 2 Setup of the ELID-assisted conditioning for coarse-grained diamond wheels

(a) Initial condition, 18μm run-out error.

(b) After 80μm infeed, 15μm run-out error.

(c) After 160μm infeed, 1.7μm run-out error.

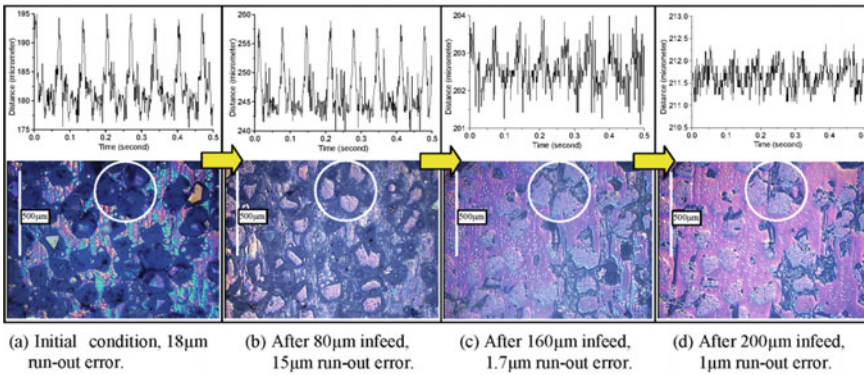(d) After 200μm infeed, 1μm run-out error.

Fig. 3 D151 coarse-grained diamond wheel run-out errors (top) and corresponding wheel topographies (bottom) [8]

depth per step of 1.5 μm, reciprocating speed of 6 mm/min, and truer speed of 1000 rpm.

Before conditioning, the run-out of coarse-grained diamond wheel exhibited a sine wave, as shown in Fig. 3a. The PV value of run-out error was about 20 μm. The run-out error decreases gradually following the conditioning process. Finally, the run-out error of 1 μm was realized after a total conditioning depth of 200 μm, which means a constant grain peripheral envelope was obtained. From the optical images, it can be found there were almost no flattened grains on the grinding wheel surface before the conditioning. As the conditioning process goes on, more and more diamond grains were truncated resulting in more flattened grain tops created. Hence, the average grain protrusion height was decreased, until the final stage shows that the bonding material was also contacted sharing the same level with the top-flattened diamond grains solidly embedded in the bonding material.

Figure 4a shows improved trend of run-out errors during the conditioning process. The changing trend of the conditioning forces is shown in Fig. 5b. Finally, the run-out errors decreased to 1.0–2.5 μm regarding different wheel peripheries from the original 16–18 μm. The change of conditioning forces, i.e., normal force F_n and
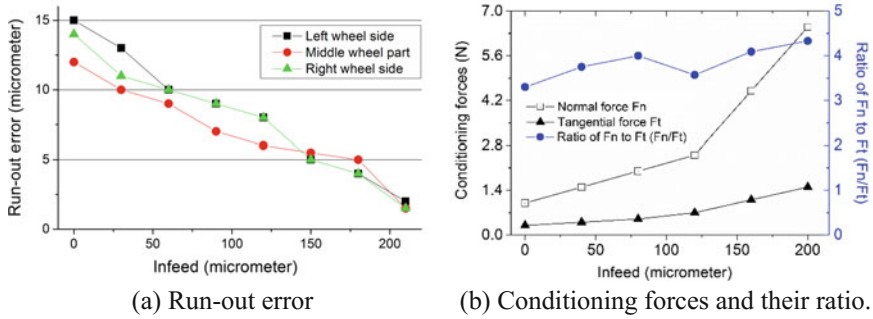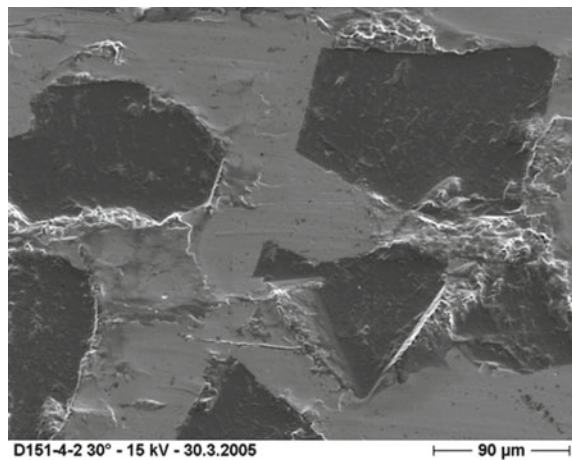
(a) Run-out error   (b) Conditioning forces and their ratio.

Fig. 4 Improvement of the D151 diamond wheel run-out error during conditioning [8]

Fig. 5 SEM images of the D151 diamond grinding wheel surface topography after the conditioning process

D151-4-2 30° - 15 kV - 30.3.2005   ⊢——— 90 µm ———⊣

tangential force Ft, as well as the force ratio Fn/Ft as a function of conditioning infeed depth is shown in Fig. 5b. As the infeed increases, both Fn and Ft increase with different speeds. Thus, the ratio Fn/Ft also increases from 3.3 to 4.35. This is caused by the increase of grain overlap rate, which means more flattened grain surfaces are generated on both the conditioning and grinding wheel, thereby creating a larger contact area between diamond grains, resulting in a bigger bearing ratio and hence larger normal forces and tangential forces. However, the tangential force does not increase as fast as the normal force; therefore, the measured increase of the ratio Fn/Ft indicates that a relatively slower truncating speed among diamond grains begins.

It can be seen from Fig. 5 that all diamond grains were conditioned with smoothly flattened top surfaces indicating that the mechanism was predominately attrition. However, there is still some tiny chipping, fracture, and cleavage present at the sides and edges of the diamond grains which are mainly attributed to the unique truncating process among super diamond abrasives, as well as the anisotropy of the diamond
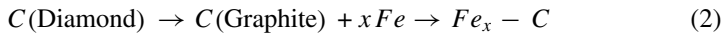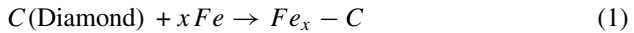
grains. Another very important aspect of the conditioning process is that there is no shedding (pullout) of diamond grains, since the grains are held strongly by a tough electroplated bonding material.

In conclusion, the on-site conditioning technique using ELID for D151 diamond wheels with the optimized conditioning parameters was able to generate a grinding wheel run-out error less than 2 μm, a constant grain peripheral envelope, and a flattened diamond grain top surface. It proves that this conditioning technique is applicable and feasible for conditioning coarse-grained diamond wheels.

2.2 *Thermochemical Conditioning of Coarse-Grained Grinding Wheels*

The above-mentioned ELID-assisted conditioning with metal bond diamond truer definitely requires the additional ELID equipment. Furthermore, the ELID electrolyte coolant is considered to erode the machining tool. Therefore, the thermochemical conditioning with metal truer was developed for coarse-grained grinding wheels further, in order to expand the application of coarse-grained grinding wheels.

Generally speaking, the thermochemical action is an important reason for diamond abrasive wear when machining steel materials. During the machining process, the chemical affinity interaction between iron and carbon atom could occur as follows [10]

$$C(\text{Diamond}) + xFe \rightarrow Fe_x - C \tag{1}$$

$$C(\text{Diamond}) \rightarrow C(\text{Graphite}) + xFe \rightarrow Fe_x - C \tag{2}$$

Diamond could succumb to graphitization at higher machining temperature due to its metastable feature. Therefore, the conversion from diamond to graphite becomes fast. Moreover, at the contact area between diamond and steel, the carbon atoms would penetrate to steel. The strong affinity between carbon and iron exacerbates the diffusion motion. In this process, the carbon atoms spread to and fill the vacancies in the metal lattice. In addition, the micro-collapse mechanical crushing also contributes to the diamond grit wear. Stress concentration results in that the specific cutting force may exceed the breaking strength of the diamond grits, and then the different forms of mechanical micro damage appear on the diamond grits. It suggests that the diamond wear mechanisms are mainly chemical reactions, diffusion motion, and mechanical factors when machining steel materials. This means steel would be the conditioning tool for coarse-grained diamond wheel.

Based on the above-mentioned analysis, the D151 electroplated coarse-grained diamond grinding wheel with a diameter of 200 mm was conditioned using the Cr12 steel by dry grinding process. Figure 6 shows the conditioning setup and the schematic diagram. SiC block was used for sharpening the clogging grinding wheel in conditioning process.
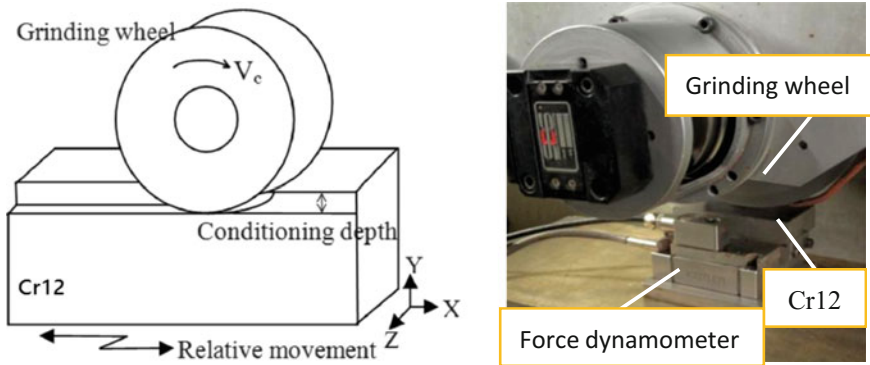
Fig. 6 Set-up of the thermochemical conditioning for coarse-grained diamond wheels
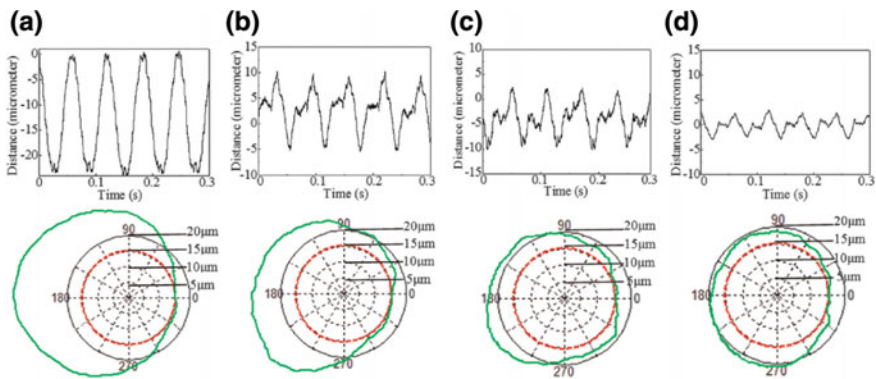

Fig. 7 Run-out error curves (top) and peripheral contour (bottom): **a** before conditioning, **b** conditioning for 2 h, **c** conditioning for 4 h, and **d** conditioning for 6 h [11]

During the conditioning, the run-out error of grinding wheel was measured, as shown in Fig. 7. The initial run-out error was mainly derived from the wheelbase manufacturing error and installation deviation. Following the conditioning, the measured circumferential contour became increasingly close to the ideal profile. The affinity interaction and chemical reactions between iron and carbon would occur on the contact area, which thus accelerate the conditioning speed.

Figure 8 shows the diamond grit morphology before and after conditioning. After conditioning, the diamond abrasive tips were flattened for reducing the run-out error. For the diamond grit A, the stress concentration that led to the abrasive internal stress was close to or even exceeded its fracture strength. Consequently, there generated the sectional micro-crushing, which would be beneficial to avoid the violent collision with the workpiece surface in the subsequent grinding. While for the grit B, the diamond tip was gradually blunt, and a widening abrasion plane perpendicular to
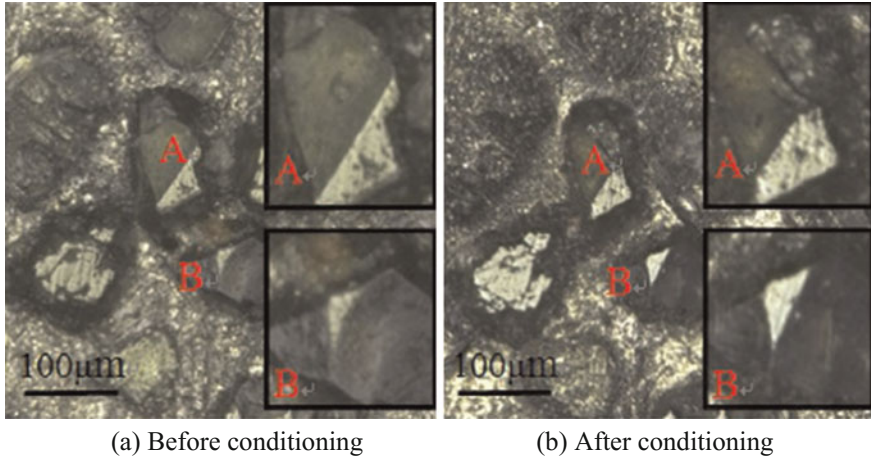
(a) Before conditioning   (b) After conditioning

Fig. 8 Comparison of diamond grit morphology before and after conditioning [11]
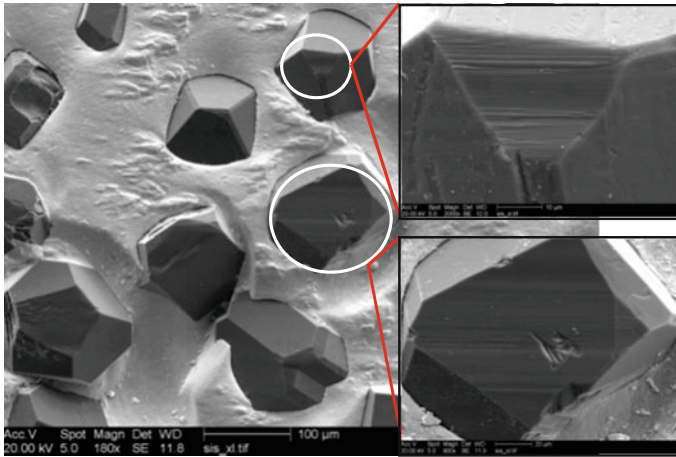

Fig. 9 Surface morphology of conditioned grinding wheel by SEM

the wheel radius direction was then formed. The detail of surface morphology of conditioned grinding wheel is shown in Fig. 9.

Raman spectra results have significant differences for various kinds of carbon materials. The Raman peaks at 1327 and 1582 cm^{-1} characterize sp3-hybridized diamond and sp2 hybrid graphite, respectively, and the spectral peak of Fullerene C60 is at 1469 cm^{-1} [12]. Figure 10a and b shows the laser Raman spectroscopy of the diamond abrasive surface before and after conditioning. After conditioning, graphite and C60 substances were generated on the abrasive surface. While the diamond and C60 substances were also found on Cr12 steel surface, as shown in Fig. 10c. That
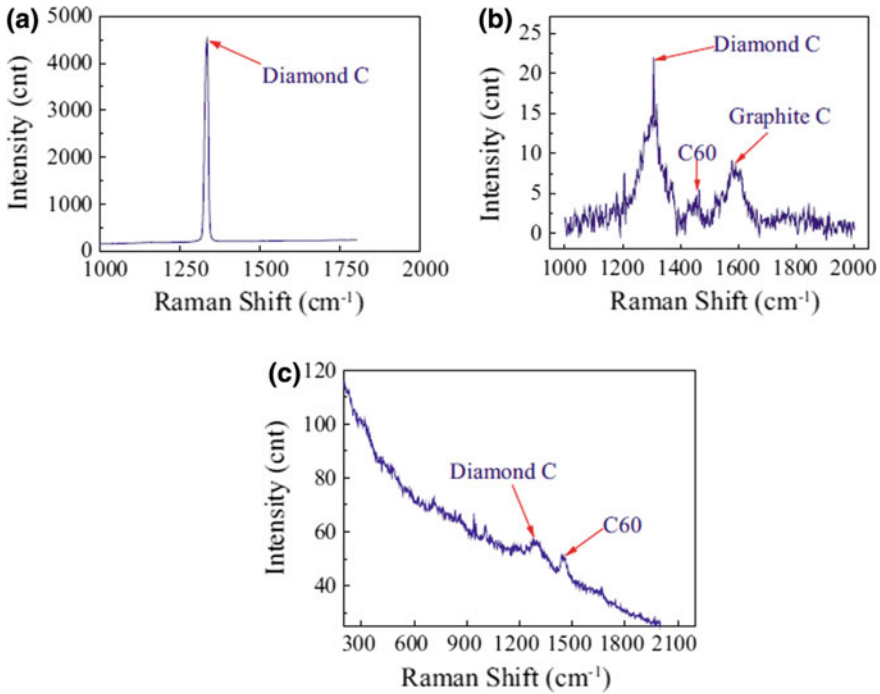
Fig. 10 Raman spectra results of abrasives and truer: **a** before conditioning (abrasive), **b** after conditioning (abrasive), and **c** after conditioning (truer) [11]

was caused by the affinity action between diamond abrasive and steel truer, as well as by the carbon atoms of abrasive gradually migrating and permeating to the truer.

It can be concluded that the electroplated coarse-grained diamond wheel could be effective and precision conditioned by the thermochemical conditioning with Cr12 metal truer. The run-out error quickly converged to 5.8 μm. Graphite and C60 were generated on the conditioned abrasive surface, showing that the conditioning mechanism is mainly involved in passivation, oxidation, and diffusion wear, as well as in a small amount of micro-crushing. It should be noted, however, the conditioning time was much longer than the ELID-assisted conditioning with metal bond diamond truer. Moreover, the thermal deformation of grinding wheel caused by conditioning heat would limit the further enhancement of conditioning accuracy.

2.3 Mechanical Conditioning of Coarse-Grained Grinding Wheels

In order to cover the problems of above-mentioned conditioning methods, an on-site mechanical conditioning of coarse-grained diamond wheels was developed. The metal truer was replaced by vitrified bond diamond truer. Figure 11 shows the experimental setup for precision conditioning of coarse-grained diamond wheel. The 1A1-type electroplated coarse-grained diamond wheel with grit size of D213 was adopted in this experiment. The grinding wheel has the specification of diameter 75 mm and width 3 mm. The conditioning process was performed on a precision plane grinder. An additional precision spindle was fixed as the grinding spindle. The hydrostatic spindle of grinder was used as the conditioning spindle. The vitrified diamond truer (grain size of 75 μm) was adopted for realizing the conditioning of coarse-grained diamond wheel. The outer diameter of the truer is 180 mm, and the width of the conditioning area is 25 mm. The radial run-out of grinding wheel and the wheel-truer contact state was measured by on-site laser displacement sensor and online acoustic emission (AE) sensor, respectively. The consistent parameters including 5000 rpm grinding wheel speed, 100 rpm truer speed, 50 mm/min reciprocating speed, and 1 μm per pass truing depth were used in the experiments.

The surface morphology of electroplated coarse-grained before and after conditioning is shown in Fig. 12. The original diamond wheel surface morphology exhibited embedded diamond grains with different geometries and different protrusion heights, which would lead to the brittle fracture of hard and brittle materials. Figure 12b indicates the conditioned wheel surface by vitrified diamond truer with 180 μm truing depth. The micro-cleavage, fracture, and flat top surfaces were generated on the diamond grains. Compared with the conditioning method with metal bond diamond truer and ELID, the conditioning process was operating in a more steady state. The conditioning was never interrupted due to the friability and self-
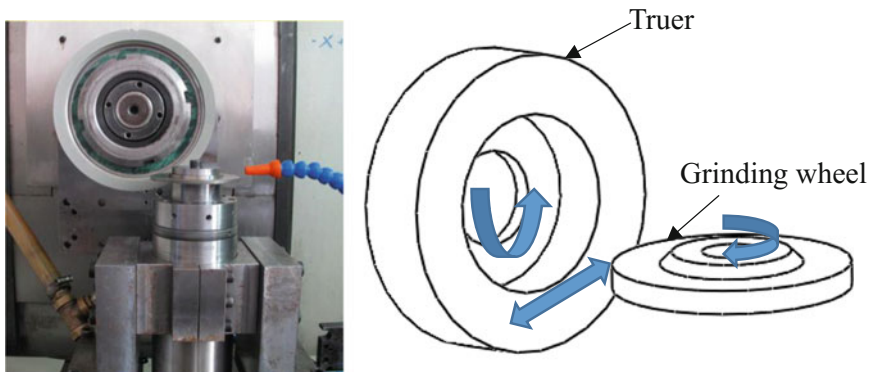

Fig. 11 Conditioning experimental setup of coarse-grained diamond wheel

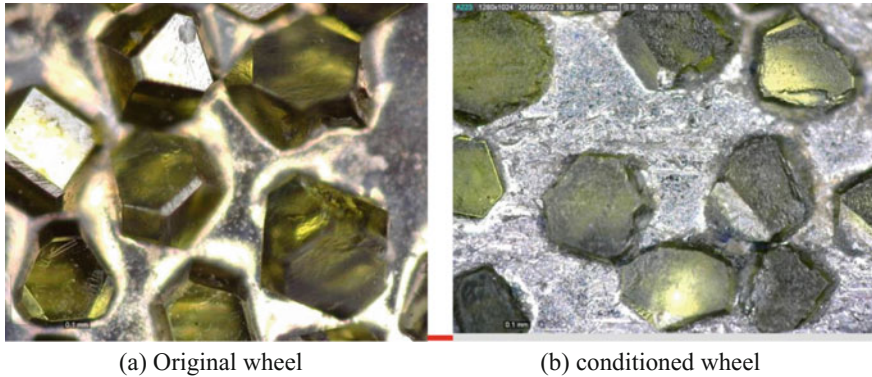(a) Original wheel   (b) conditioned wheel

Fig. 12 Surface morphology of D213 diamond wheels

sharpening of vitrified truer. The conditioning cost time was reduced to less than 3 h, and any additional equipment was not to be required.

To determine the conditioning threshold value of coarse-grained diamond wheel for realizing the ultra-precision grinding, the influences of the truing depth on ground surface quality, grinding wheel run-out was investigated. The BK7 glass workpiece was grounded with the grinding parameters (5000 r/min, 30 mm/min, 2 µm) after every 30-µm truing depth, as shown in Fig. 13. It reveals that the truing depth had an important influence on the ground surface topography. As described in Fig. 13a, there were obvious groove profiles and the brittle removed areas on the ground surface obtained by original coarse-grained diamond wheel, which means the material was removed mainly in brittle regime. As the truing depth increased from 30 to 120 µm, the surface groove depth and the brittle removed areas were decreased gradually, while ductile removed areas, on the contrary, were increased. When the truing depth increased to 150 µm, the workpiece surface was completely machined in ductile regime, as shown in Fig. 13f. There is no brittle crack, and grinding traces were observed on the ground surface. The surface roughness Ra values in the vertical and parallel to the grinding direction were less than 4 and 2 nm, respectively. The precision grinding of optical glass with nanometer-scaled surface roughness was realized.

In the previous conditioning experiments, the radial run-out of grinding wheel is a common judgment method for conditioning process, which is the same as that of fine-grained grinding wheels. However, grinding experimental results (as shown in Fig. 13) indicated the conditioned wheels with large run-out error could also often yield ductile ground surface with nanometer scale roughness. This proves for coarse-grained diamond wheel, the profile accuracy of contour circle which consists of well-conditioned diamond grit flat tops is the key for realization of precision grinding, but not the run-out error. For the run-out error of coarse-grained diamond wheel, not only the abrasive grains but also the bond surface between grains would contribute to the run-out measured results. When the diamond grain tops have been truncated
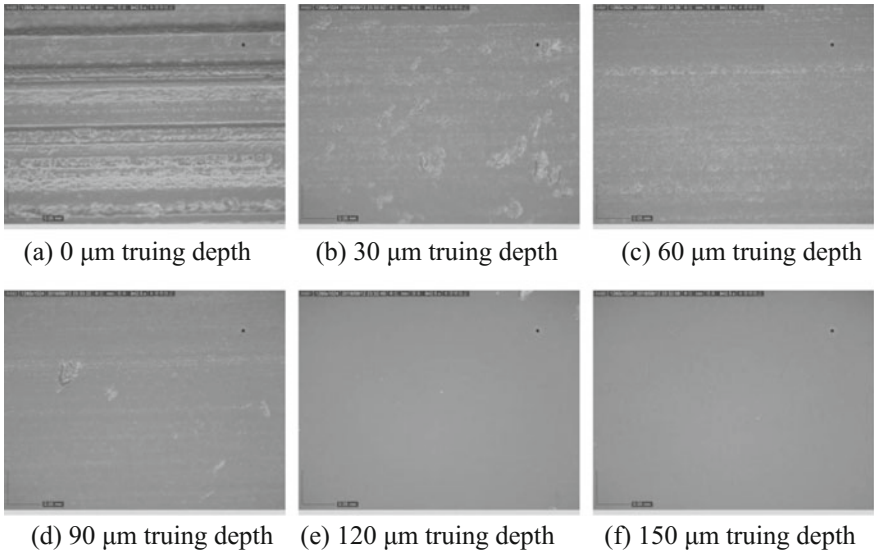
(a) 0 μm truing depth   (b) 30 μm truing depth   (c) 60 μm truing depth

(d) 90 μm truing depth   (e) 120 μm truing depth   (f) 150 μm truing depth

Fig. 13 Ground surface morphology by conditioned wheels with different truing depths (×900)
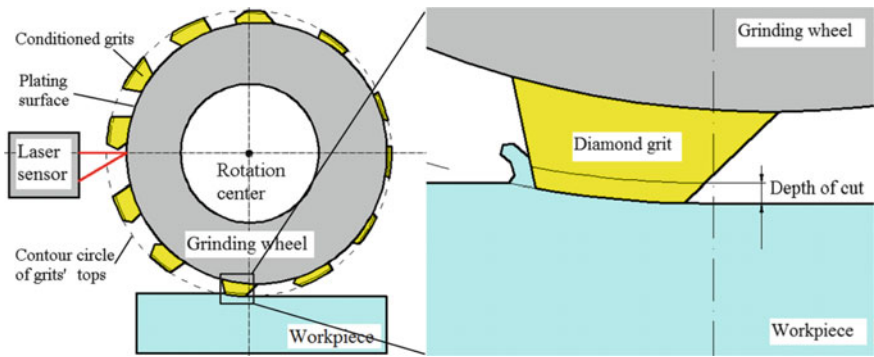
Fig. 14 Illustration of conditioned coarse-grained diamond wheel and the relation between grinding wheel run-out and depth of cut [13]

into a satisfactory contour circle, the radial run-out of grinding wheel was mainly determined by the variation of grit protrusion height from bond surface of wheel, as shown in Fig. 14 [13]. Therefore, the run-out error of coarse-grained diamond wheel would not be limited in microns like the conventional fine-grained wheel, unless the coarse-grained diamond grains are totally truncated off along the lowest plating surface resulting in a minimized run-out error within 2 μm, as presented by Zhao and Guo [8].

The effect of truing depth on the radial run-out of different surface positions of grinding wheel is shown in Fig. 15a. It reveals that the truing depth has a serious

(a) grinding wheel run-out error   (b) conditioning AE signal

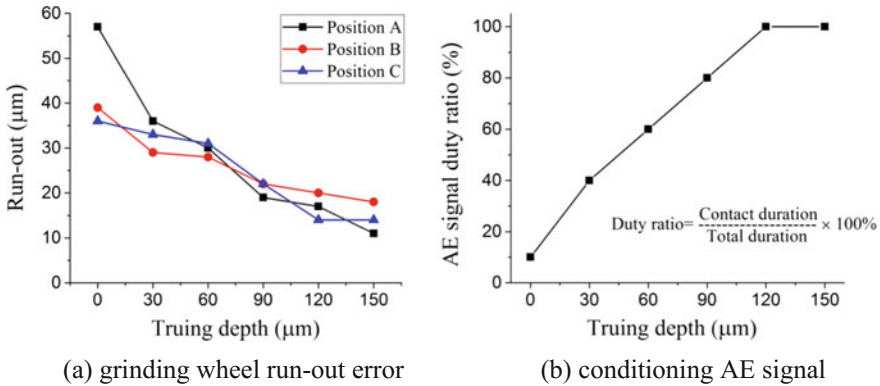**Fig. 15** Effects of truing depth on grinding wheel run-out and conditioning AE signal

influence on grinding wheel run-out. The run-out values of different positions were reduced gradually with the increase of truing depth. The run-out of original wheel was 35–60 µm caused by both of wheel manufacture error and of wheel installation error. The diamond wheel run-out values after truing depth of 120 and 150 µm were 14–20 and 11–18 µm, respectively. That means that, unlike fine diamond wheel conditioning, the run-out values' deviation of different wheel surface positions was not converged at the end of conditioning process. In other words, the run-out variation caused by measure position was more than that by truing depth, which resulted from the irregular conditioned wheel surface. Therefore, the radial run-out of grinding wheel is hard to be selected as the conditioning evaluation parameter.

Compared the radial run-out, the AE signal judgment method of grinding wheel conditioning is more sensitive and can be measured online [14]. The relationship between truing depth and AE signal of conditioning process is shown in Fig. 15b. In the beginning of conditioning, the AE signal duty ratio was approximately equal to 10%, which implies only about 10% surface of diamond wheel was contacted with truer. As the conditioning process goes on, the AE signal duty ratio was increased, which means increasing surface of grinding wheel did contact with truer and more and more diamond grains were conditioned and truncated. It should be noted that the AE duty ratio reached 100%, when the truing depth was 120 µm. According to Fig. 13e, however, the conditioned coarse-grained diamond wheel with 120 µm truing depth did not realize entirely ductile precision grinding. This was because that the AE measurement method used in this experiment only indicated the peripheral conditioning status of diamond wheel, but the axial conditioning status could not be estimated by AE signal duty ratio. The axial deviation of grain protrusion height would also result in the cracks and brittle material removal in plane grinding. Therefore, an additional conditioning process with truing depth of 30 µm was carried out after the AE signal duty ratio was reached to 100%.

In conclusion, three kinds of conditioning technique were adopted for conditioning coarse-grained diamond wheels including electrolytic in-process dressing

(ELID)-assisted conditioning with metal bond diamond truer, thermochemical conditioning with metal truer, and mechanical conditioning with vitrified diamond truer. The experimental results indicated that all of three kinds of conditioning technique are applicable and feasible for conditioning coarse-grained diamond wheels, in order to realize the ultra-precision grinding of hard and brittle materials. In addition, the judgment method of grinding wheel conditioning was investigated. Compared with run-out error, the AE single is more suitable to be adopted as judgment parameter in the conditioning process of coarse-grained diamond wheels.

3   Ultra-precision Grinding of Hard and Brittle Materials

In order to solve the problems of wheel loading and wheel wear, avoid the periodic conditioning requirement of the fine-grained diamond wheels (grain size from several microns down to submicron scale), and achieve high-efficiency precision grinding of optical glasses, the deterministic grinding process with coarse-grained diamond wheels featuring grain sizes of approx. 90–300 μm have been paid more attention [15–17]. Prior to the grinding process, the protuberances of the diamond coarse grains have to be truncated with the specific conditioning method, aiming to guarantee diamond grains with a constant wheel peripheral envelope surface. Here, the ultra-precision grinding of hard and brittle materials with coarse-grained grinding wheels was investigated in order to reveal the performance of these coarse-grained grinding wheels.

3.1   Ductile Grinding Mechanism of Conditioned Coarse-Grained Wheels

In order to realize the ductile and precision grinding on hard and brittle materials by conditioned coarse-grained diamond grinding wheel, the maximum undeformed chip thickness must be less than the critical ductile–brittle transition depth of workpiece material. Unlike the conventional fine-grained wheel, in grinding process with a conditioned coarse-grained grinding wheel, the material is removed by the truncated abrasive grains. The characteristic chip shape for a truncated abrasive grain is shown in Fig. 16.

   The chip cross-sectional profile is trapezoid. The chip width is determined by average grain cutting length b_s. The maximum undeformed chip thickness h_m for truncated grains could be obtained basing on the material balance between the material removal rate and the total volume of chips produced at each effective cutting grain. The product of the average volume per chip and the number of chips formed per unit time are equal to the total volumetric removal rate [19]
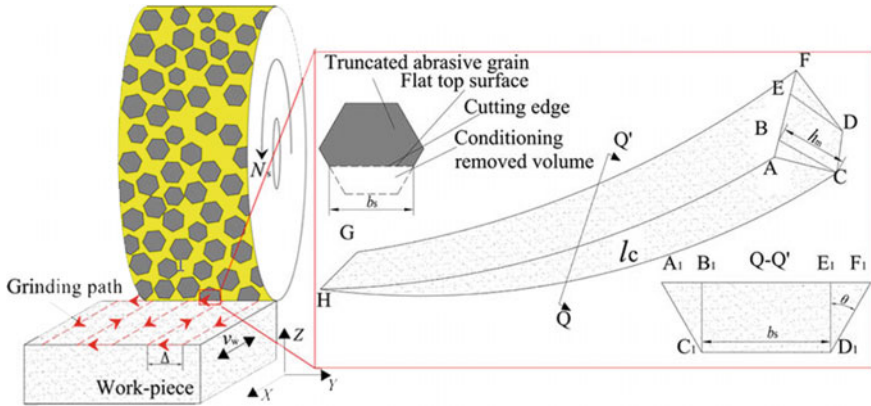
Fig. 16 Illustration of the chips generated by truncated abrasive grain [18]

$$(Cbv_s)V_c = a_p v_w b \tag{3}$$

where V_c is the average volume per chip, C is the grain density on the wheel surface, v_s is the grinding speed, v_w is the feed rate, and a_p is the grinding depth. Thus, (Cbv_s) is the number of chips per unit time for the whole wheel width b and $(a_p v_w b)$ is the theoretical volumetric removal rate.

As the maximum undeformed chip thickness h_m is much smaller than the abrasive cutting chip length l_c [19],

$$l_c = \sqrt{a_p \cdot d_s} \tag{4}$$

where d_s is equivalent wheel diameter.

As distinctly illustrated in Fig. 16, the chip could be divided into three parts: the pyramid BCDEHG and two tetrahedrons ABCH and DEFG.

$$V_c = V_{\text{BCDEGH}} + V_{\text{ABCH}} + V_{\text{DEFG}} \tag{5}$$

Hence, the chip volume for a truncated abrasive grain can be expressed by

$$V_c = b_s \cdot h_m \cdot l_c / 2 + h_m^2 \cdot \tan \theta \cdot l_c / 3 \tag{6}$$

where θ is the inclination angle of the abrasive grain side edge ($\theta > 0$).

Substituting the chip volume and the cutting chip length into Eq. (3), we can obtain the theoretical maximum undeformed chip thickness h_m for grinding process with conditioned coarse-grained wheel, as:

$$h_{\mathrm{m}} = -\frac{3b_s}{4\tan\theta} + \frac{1}{2}\left[\left(\frac{3b_s}{2\tan\theta}\right)^2 + \frac{12}{C\tan\theta}\left(\frac{v_w}{v_s}\right)\left(\frac{a_p}{d_s}\right)^{1/2}\right]^{1/2} \tag{7}$$

Table 1 Material properties of typical hard and brittle materials

Material	Vickers hardness H/GPa	Elastic modulus E/Gpa	Fracture toughness K_{IC}/Mpa·m$^{-1/2}$
SiC	28	410	4.5
WC	26.4	680	5.3
Zerodur	6	91	2.6
BK7	5.7	88.5	0.72

Here, b_s is set as 200 µm according to the average measurement value of conditioned diamond wheel with D213 µm abrasive size, θ is set as 35.3° in view of the abrasive grain shape [20], C is the grain density on wheel surface, and is 10.93/mm^2 for D213 µm wheel based on the experimental measurement.

The critical depth of cut for ductile machining hard and brittle materials could be determined by Bifano [21]

$$d_c = 0.15 \cdot \left(\frac{E}{H} \right) \cdot \left(\frac{K_{IC}}{H} \right)^2 \tag{8}$$

where E is the elastic modulus, H is the Vickers hardness, and K_{IC} is the fracture toughness. The material properties of typical hard and brittle materials are listed in Table 1. The calculated critical depths for SiC ceramic, WC cement, Zerodur glass ceramic, and BK7 optical glass are 60.2, 156, 91, and 37 nm, respectively.

As shown in Fig. 17, the chip thickness increases sharply with the feed rate. In contrast, the chip thickness exhibits an opposite tendency to the grinding wheel rotation. The ductile–brittle transition depth for BK7 is only 37 nm, so the grinding parameters for traverse surface grinding could be set at a rotation of 5000 r/min, feed rate of 50 mm/min, grinding depth of 2 µm. In the same way, the grinding parameters of 5000 r/min, 1.0 mm/min, and 5.0–25.0 µm could be used for ductile machining SiC. The corresponding h_m is less than 1.2 nm, which is adequate to generate the ground surface in ductile machining regime.

3.2 Ground Surface Quality by Conditioned Coarse-Grained Diamond Wheels

The ultra-precision grinding of BK7 optical glass with different grinding wheels including D151 conditioned coarse-grained grinding wheel, D7 fine-grained resin grinding wheel, and D7 fine-grained metal grinding wheel with ELID technology was investigated. The workpiece was 180 mm × 160 mm × 40 mm. The grinding parameters were 1600 r/min spindle speed, 1 µm depth of grinding, and 200 mm/min feed rate. The experimental setup is shown in Fig. 18.
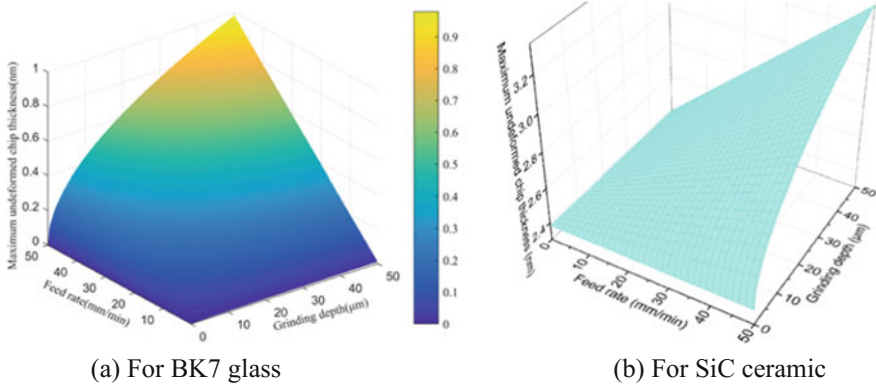
(a) For BK7 glass   (b) For SiC ceramic

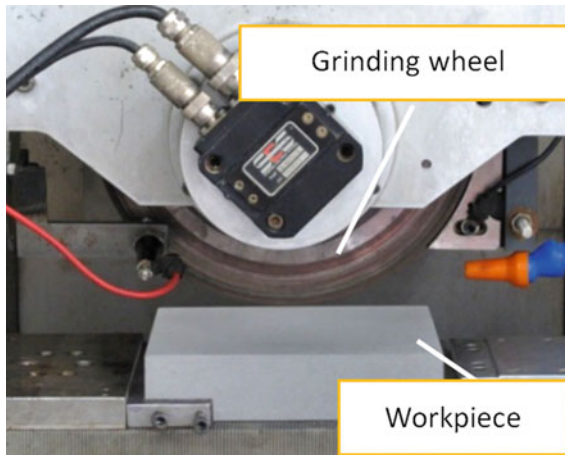**Fig. 17** Calculation of the maximum undeformed chip thickness

Fig. 18 BK7 glass grinding device

The grinding wheel's wear volume and grinding ratio with the same grinding parameters are shown in Fig. 19. Under the same glass removal volume of 14,400 mm^3, the wear volume of fine-grained resin grinding wheel, fine-grained metal grinding wheel, and conditioned coarse-grained grinding wheel was 2837.07, 2024.23, and 41.6 mm^3, respectively. Figure 19b indicates the grinding ratio which equals to the workpiece material removal volume divided by the grinding wheel's wear volume. The grinding ratio of fine-grained resin grinding wheel, fine-grained metal grinding wheel, and conditioned coarse-grained grinding wheel was 5.08, 7.11, and 346.16, respectively. The grinding ratio of conditioned coarse-grained grinding wheel was 50–70 times of that of fine-grained grinding wheels. This means that the conditioned coarse-grained grinding wheel has much greater wear resistant.
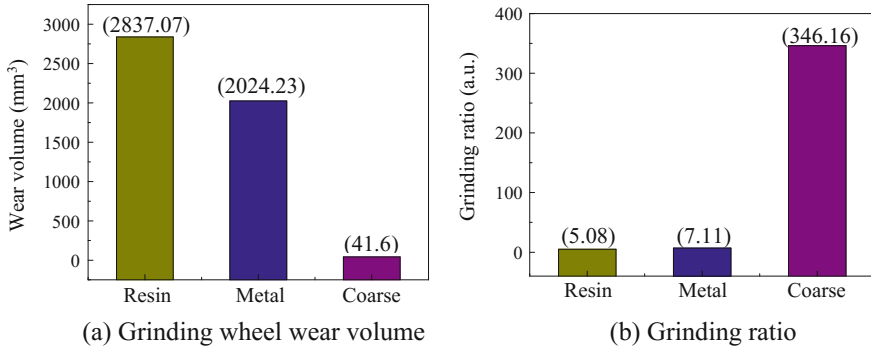
Fig. 19 Grinding wheel's wear volume and grinding ratio under the same glass removal volume. Resin: D7 fine-grained resin grinding wheel; metal: D7 fine-grained metal grinding wheel with ELID technology; and coarse: D151 conditioned coarse-grained grinding wheel
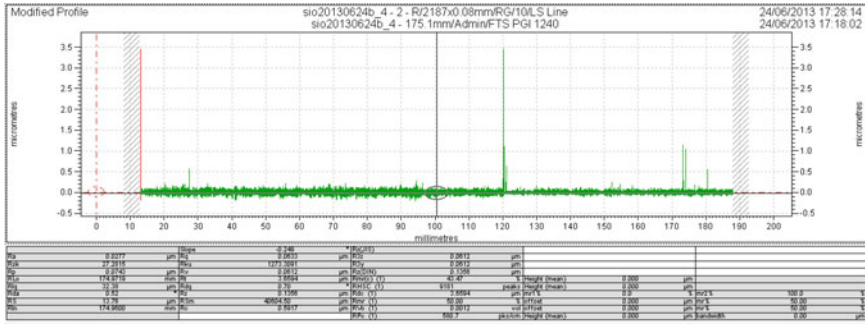
The roughness of ground surface with conditioned coarse-grained grinding wheel in different measurement directions by profilometer is shown in Fig. 20. Parallel to the grinding direction, the roughnesses Ra and Rq were 27.7 and 63.3 nm, respectively, while the roughnesses Ra and Rq were 54.1 and 110.5 nm in the perpendicular direction.

Figure 21 shows the ground surface roughness by different grinding wheels. The measure results indicated that, compared with the conventional fine-grained diamond wheels, the conditioned coarse-grained grinding wheel could obtain same ground surface roughness.

The form accuracy of ground surface with conditioned coarse-grained grinding wheel in different measurement directions by profilometer is shown in Fig. 22. Parallel to the grinding direction, the form accuracy PV was 2.28 μm in 175 mm measure distance, while the form accuracy PV was 4.17 μm/155 mm in the perpendicular direction.

Figure 23 shows the PV values compared results of ground surface with three different grinding wheels. It was found that the form accuracy with conditioned coarse-grained grinding wheel was significantly lower than the other fine abrasive grinding wheels. This is because, during the grinding process, the diamond abrasive grains of the fine abrasive grinding wheel were relatively easy to fall off, while the coarse-grained grinding wheel had a stronger holding force. Therefore, the preservation of form accuracy was better.

Furthermore, the grinding experiments were carried out on BK7 and Zerodur with three coarse-grained diamond wheels of three different grain sizes in order to further reveal the performance of these coarse-grained grinding wheels. The feed rate applied to BK7 was 4 mm/min, while for Zerodur was 10 mm/min. Prior to the grinding tests, the workpiece was grounded and polished in order to guarantee the good flatness, low surface roughness, and free subsurface damage.

(a) Parallel to the grinding direction
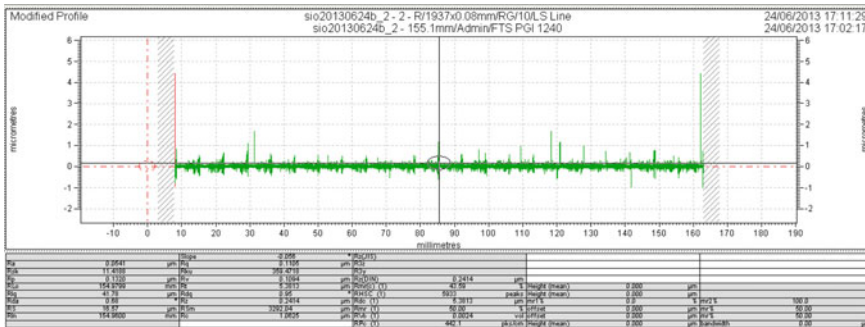
(b) Perpendicular to the grinding direction

Fig. 20   Surface roughness of BK7 ground by conditioned coarse-grained grinding wheel
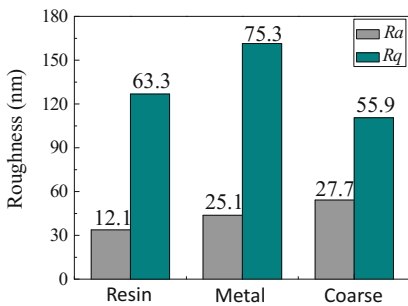
(a) Parallel to the grinding direction
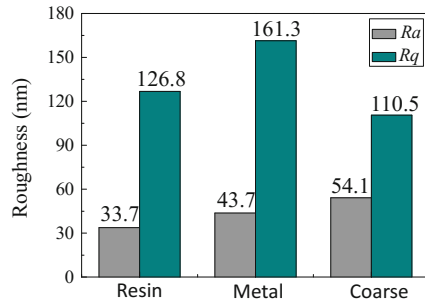
(b) Perpendicular to the grinding direction

Fig. 21   BK7 glasses' surface roughness results of each direction. Resin: D7 fine-grained resin grinding wheel; metal: D7 fine-grained metal grinding wheel with ELID technology; and coarse: D151 conditioned coarse-grained grinding wheel

(a) Parallel to the grinding direction

(b) Perpendicular to the grinding direction

Fig. 22 Surface form error results of BK7 glasses ground by conditioned coarse-grained grinding wheel

(a) Parallel to the grinding direction

(b) Perpendicular to the grinding direction

Fig. 23 Ground surface form accuracy

Ra: 34.68nm, Rq: 42.83nm, PV: 148.7nm | Ra: 19.42nm, Rq: 26.16nm, PV: 120.7nm | Ra: 15.47nm, Rq: 18.08nm, PV: 104.1nm

Ra: 11.66nm, Rq: 14.34nm, PV:115.5nm | Ra: 8.72nm, Rq: 11.36nm, PV: 78.85nm | Ra: 3.94nm, Rq: 4.69nm,PV: 40.80nm

(a) Top: WLI image of the surface ground with a D46 grinding wheel. Bottom: AFM image of the area marked in the WLI image.

(b) Top: WLI image of the surface ground with a D91 grinding wheel. Bottom: AFM image of the area marked in the WLI image.

(c) Top: WLI image of the surface ground with a D151µm grinding wheel. Bottom: AFM image of the area marked in the WLI image.
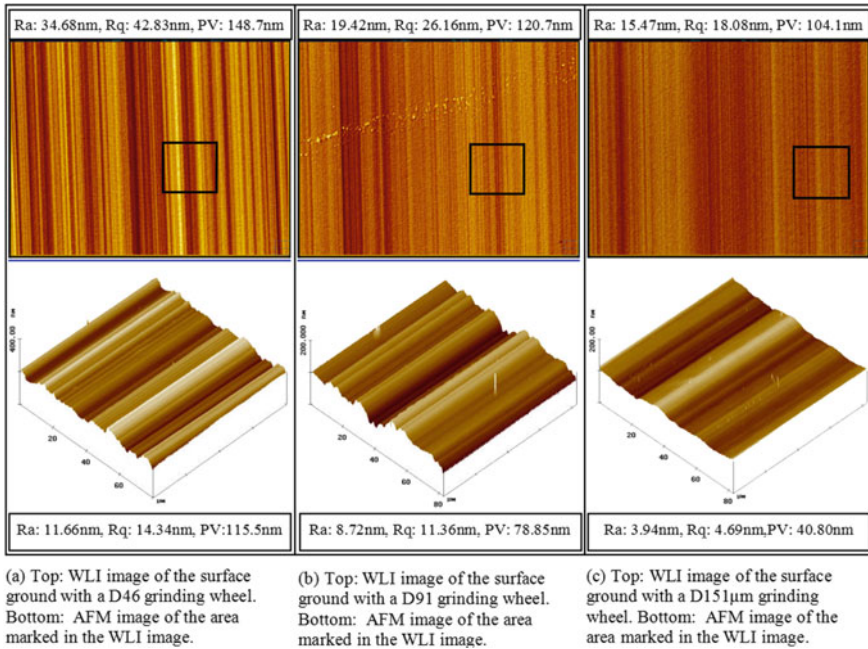
Fig. 24 WLI (top) and AFM (bottom) images of ground surface with conditioned D46 (**a**), D91 (**b**), and D151 (**c**) diamond wheels with a feed rate of 10 mm/min and a depth of cut of 3 µm [15]

From Fig. 24(a, top), it can be seen that the ground BK7 surface had a surface roughness of 148.7 nm (PV) or 34.58 nm (Ra) as measured with a WLI, indicating a non-uniformity of protruding diamond grain heights of the grinding wheel over a length of 404.64 µm in axial direction. According to the AFM image shown in Fig. 24(a, bottom), over a scanned range of 80 µm × 80 µm, the corresponding surface roughness was 11.656 nm (Ra) or grain height non-uniformity was 115.5 nm (PV). Both WLI and AFM images proved that the precision-conditioned grinding wheel was capable of carrying out ductile grinding of BK7. From Fig. 24b, it can be seen that the ground BK7 with D91 wheel shared the similar surface topography with that ground by the 46 µm grain size diamond wheel, except the smaller surface roughness either in PV 120.7 nm by WLI and 78.85 nm by AFM, or in Ra 19.42 nm by WLI and 8.72 nm by AFM under the identical scanned ranges. This result indicated that the precision-conditioned 91 µm grain size diamond wheel was capable of realizing ductile grinding of BK7 with a smaller surface roughness when compared to 46 µm grain size diamond wheel. According to Fig. 24c, the ground BK7 surface by D151 wheel exhibits the smallest surface roughness (WLI, PV: 104.1 nm, Ra: 15.47 nm; AFM, PV: 40.8 nm, Ra: 3.94 nm) among that ground by three different grain size diamond wheels. There are also copied grinding marks from the wheel without cracks distributed on the ground surface, indicating a ductile grinding mode is mainly involved during the grinding process.
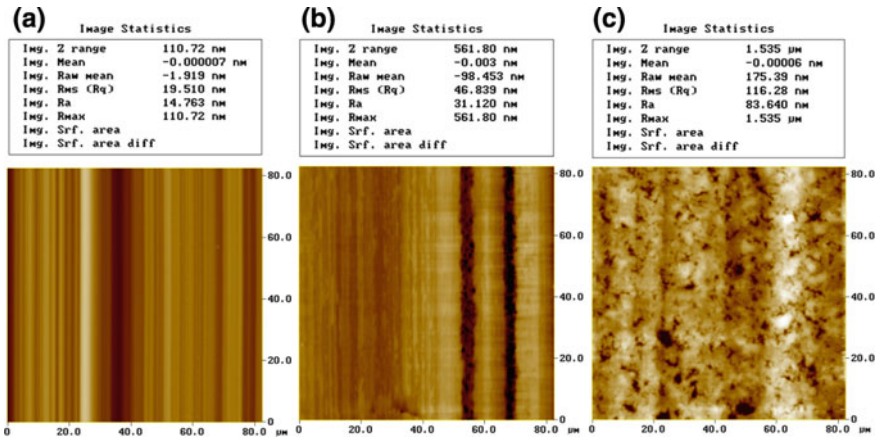
(a) Image Statistics

Img. Z range	110.72 nm
Img. Mean	-0.000007 nm
Img. Raw mean	-1.919 nm
Img. Rms (Rq)	19.510 nm
Img. Ra	14.763 nm
Img. Rmax	110.72 nm
Img. Srf. area	
Img. Srf. area diff	

(b) Image Statistics

Img. Z range	561.80 nm
Img. Mean	-0.003 nm
Img. Raw mean	-98.453 nm
Img. Rms (Rq)	46.839 nm
Img. Ra	31.120 nm
Img. Rmax	561.80 nm
Img. Srf. area	
Img. Srf. area diff	

(c) Image Statistics

Img. Z range	1.535 µm
Img. Mean	-0.00006 nm
Img. Raw mean	175.39 nm
Img. Rms (Rq)	116.28 nm
Img. Ra	83.640 nm
Img. Rmax	1.535 µm
Img. Srf. area	
Img. Srf. area diff	

Fig. 25 Grinding of Zerodur with conditioned D46 diamond wheel and different depths of cut: **a** depth cut of 10 µm, **b** depth cut of 5 µm, **c** depth cut of 60 µm [15]

From the above results, it can be concluded that all three precision-conditioned grinding wheels were able to carry out ductile grinding of BK7. The D151 wheel generated surface features with the smallest roughness and lowest PV value, while the D91 and D46 wheels generated surfaces feature with relatively higher roughness and bigger PV value. This fact shall be resulted by the different overlap ratios exhibited by different coarse-grained diamond grinding wheels. D151 wheel has the biggest overlap ratio, while the D46 wheel has the smallest one.

From Fig. 25(a, left), it can be seen that under a depth of cut of 10 µm, the ground Zerodur surface with D46 diamond wheel exhibited a crack and fracture-free morphology resulted from a total ductile material removal mode, featuring a PV value of 110.72 nm and Ra of less than 15 nm. As the depth of cut increased to 15 µm, the ground Zerodur surface morphology became to present the cracks and fractures alongside with the ground groves. The ground morphology indicated a mixed ductile and brittle materials removal mode, resulting in a much big surface roughness values, as shown in Fig. 25b. While as shown in Fig. 25c, when the depth of cut finally reached to 60 µm, the ground Zerodur surface showed no similar morphology as indicated in Fig. 25a, b but fully distributed with propagated cracks and pits. The results indicated that the conditioned D46 wheel was capable of realizing ductile material mode grinding of Zerodur when the depth of cut was set in between 10 and 15 µm, at a feed rate of around 10 mm per minute.

When the same grinding parameters as of D46 wheel were applied to D91 wheel, the resulted surface quality (refer Fig. 26) was better than that resulted from D46. Under both depths of cuts of 10 and 15 µm, the ground Zerodur surfaces were totally of ductile material removal mode featuring grinding marks and quite small surface roughness values (PV of about 30 nm while Ra of about 4 nm). When the depth of cut increased to 15 µm, the surface morphology remains similar to that under 10 µm, except the surface roughness values correspond to a big PV of about 50 nm and Ra
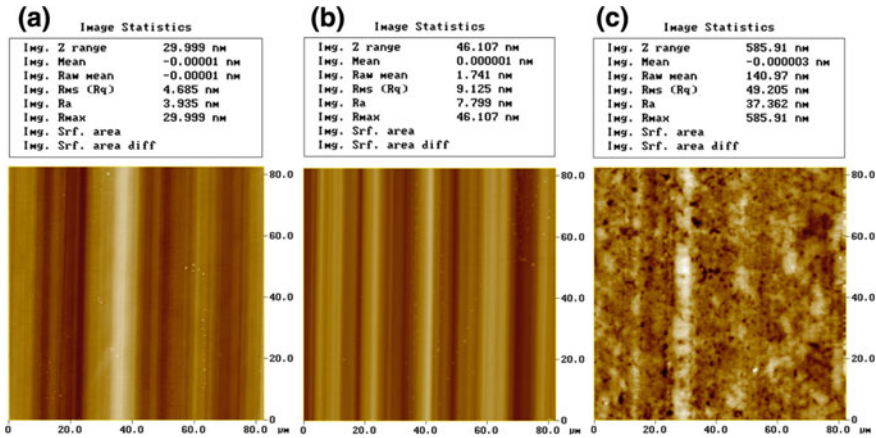
(a) Image Statistics

Img. Z range	29.999 nm
Img. Mean	-0.00001 nm
Img. Raw mean	-0.00001 nm
Img. Rms (Rq)	4.685 nm
Img. Ra	3.935 nm
Img. Rmax	29.999 nm
Img. Srf. area	
Img. Srf. area diff	

(b) Image Statistics

Img. Z range	46.107 nm
Img. Mean	0.000001 nm
Img. Raw mean	1.741 nm
Img. Rms (Rq)	9.125 nm
Img. Ra	7.799 nm
Img. Rmax	46.107 nm
Img. Srf. area	
Img. Srf. area diff	

(c) Image Statistics

Img. Z range	585.91 nm
Img. Mean	-0.000003 nm
Img. Raw mean	140.97 nm
Img. Rms (Rq)	49.205 nm
Img. Ra	37.362 nm
Img. Rmax	585.91 nm
Img. Srf. area	
Img. Srf. area diff	

Fig. 26 Grinding of Zerodur with conditioned D91 diamond wheel and different depths of cut: **a** depth cut of 10 µm, **b** depth cut of 15 µm, **c** depth cut of 60 µm [15]

of about 8 nm. This fact indicated that the conditioned D91 had a superior grinding performance for Zerodur than D46 in terms of smaller surface roughness values, as well as the total ductile material removed surface under identical depth of cuts and feed rates with D46.

In the grinding of BK7 and Zerodur using three conditioned coarse-grained diamond wheels with different grain sizes (D151, D91, and D46), the bigger the diamond grain size was, the smaller the ground surface roughness would be obtained, due to the different overlap ratios. The surface roughness achievable on BK7 and Zerodur differed due to a different machinability of these materials. However, for both BK7 and Zerodur, the ground surface roughness mainly depended on the depth of cut other than the feed rate.

3.3 Subsurface Damage by Coarse-Grained Diamond Wheels

Cross-sectional microscopy is the often used method for the measurement of subsurface damage. Optical glasses' sample preparation generally consists of four steps: cutting, lapping, polishing, and etching [15]. (1) Cutting is done in 45° to the machined surface by a diamond saw; (2) the surface of the cut sample is then polished with diamond abrasive papers to remove enough material from the inspected cross section to ensure that any damage incurred during cutting is removed; (3) the polished surface is refined by polishing with loose diamond abrasive of 1µm grain size; (4) the test surface is placed into HF acid solution (HF 5%) for 20 s at room temperature. This will make the subsurface cracks more discernible for microscopic inspection. When the sample is prepared, it needs goad coating for inspection with a scanning electron
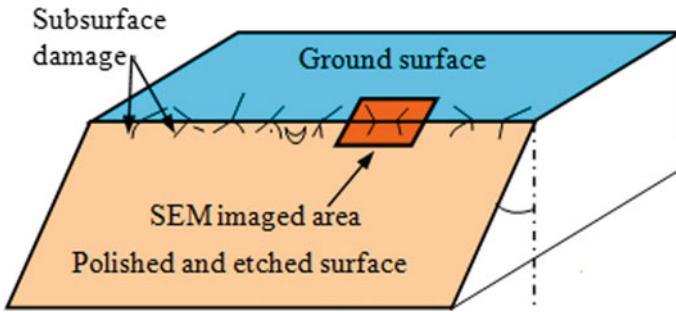
**Fig. 27** Diagram of angle polishing method [15]

(a) Low-speed sawing slicer   (b)Vacuum soaked device   (c) Polishing machine

**Fig. 28** Equipment used for sample preparation

microscope. A prepared specimen ready for SEM imaging is shown in Fig. 27. The equipment used for sample preparation is shown in Fig. 28.

The subsurface damage of ground surface by various diamond wheels are shown in Fig. 29. From Fig. 29a, it can be seen that the depth of subsurface cracks by D7 resin bond diamond grinding wheel was relatively low due to the elasticity of resin bond. The elasticity of resin bond reduced the rigid impact of the grinding wheel on workpiece. The depth of subsurface damage crack was less than 2 μm, while the depth of subsurface cracks by the D7 metal bond diamond grinding wheel was slightly larger than that by resin bond wheel because of the higher rigid of metal bond system. The depth of subsurface damage crack was about 5 μm.

Figure 29c shows the subsurface damage topography of ground surface by conditioned coarse-grained diamond wheel. It can be seen that the subsurface damage caused by conditioned coarse-grained diamond wheel was more serious than that of the fine abrasive grinding wheel, especially for BK7 glass and fused silica. The depth of subsurface damage crack was about 8 μm. In the preconditioning process, the abrasive grain protrusion height of coarse-grained diamond wheel was uniform in order to realize ductile grinding. However, the flat tops of diamond grits created in preconditioning process lead to greater specific grinding normal force. In addi-
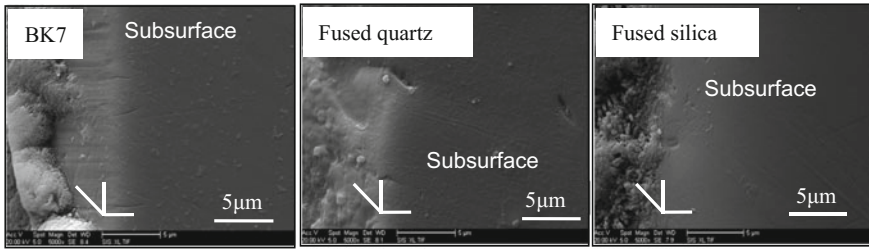
(a) Subsurface damage ground by D7 resin bonded diamond wheel
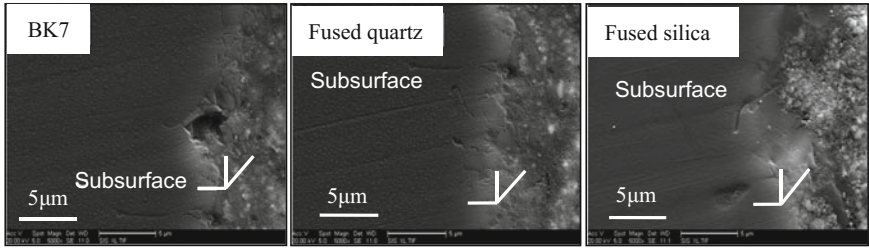
(b) Subsurface damage ground by D7 metal bonded diamond wheel
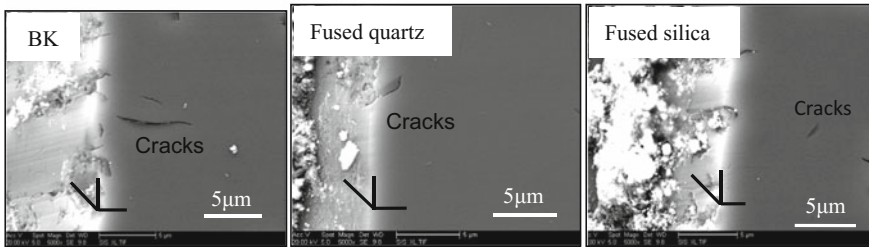
(c) Subsurface damage ground by D151 conditioned coarse-grained diamond wheel

Fig. 29 Optical glasses' subsurface damage ground by three kinds of wheels

tion, the flat tops of diamond grits did increase the friction between the workpiece and grinding wheel. Therefore, more serious subsurface damage was introduced by conditioned coarse-grained diamond wheel in grinding process.

4 Micro-structured Coarse-Grained Grinding Wheels for Improving Ground Subsurface Damage

The conditioned coarse-grained diamond grinding wheels are able to achieve the identical surface roughness, higher form accuracy, and larger material removal rate on hard and brittle materials due to their better wear resistance ability, longer grinding wheel life, and bigger chip space when compared to the traditional fine-grained

diamond wheels. However, the flat tops of diamond grits created in preconditioning process will lead to greater specific grinding normal force as presented by Heinzel and Rickens [22, 23] indicating that a serious subsurface damage will be introduced by coarse-grained diamond wheel in optical glass grinding process.

It has been shown that the micro-structured surface of diamond would reduce the normal grinding force as compared with traditional electroplate grinding block [24–26]. This is associated with the stability of active cutting elements and the integrity of micro-cutting edges composed by a number of microstructures. Besides, the increased number of cutting edges would also lead to a decrease of specific cutting force in grinding process, which can be obtained by micro-structuring of flat top diamond grits. Therefore, micro-structured diamond surface seems to have the ability to improve grinding performance of coarse-grained diamond wheels and reduce the specific grinding normal force. Based on the above, the micro-structured surface was adopted for coarse-grained diamond wheels aiming to improve the grinding performance, especially subsurface damage.

4.1   Laser Micro-structuring on Conditioned Coarse-Grained Diamond Wheel

A sub-nanosecond pulsed laser of wavelength 532 nm, pulse width 0.8 ns, pulse repetition frequency 1–5 kHz, initial laser beam diameter 3 mm, divergence angle 7 mrad, and Gaussian energy distribution was taken as the laser source for micro-structuring the diamond surface and grinding wheels. As shown in Fig. 30, the laser micro-structuring setup was composed of laser source, mirrors, focus lens, CCD cameras, laser distance sensor, and a four-axis precision translation stage. The focus lens was a $10 \times$ microscope objective and could focus the laser beam to less than $20\,\mu m$ on the focus plane.

The influence of laser power on the micro-machining of diamond material was researched with machining diamond surface, as shown in Fig. 31. Both of the groove
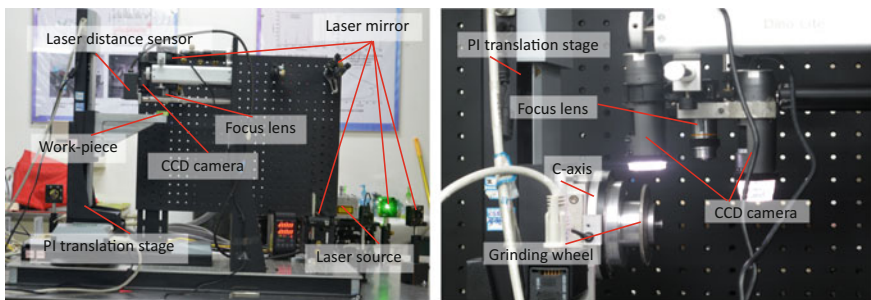

Fig. 30 Laser micro-machining setup

(a) diamond groove morphology   (b) 70 mW enlarged image

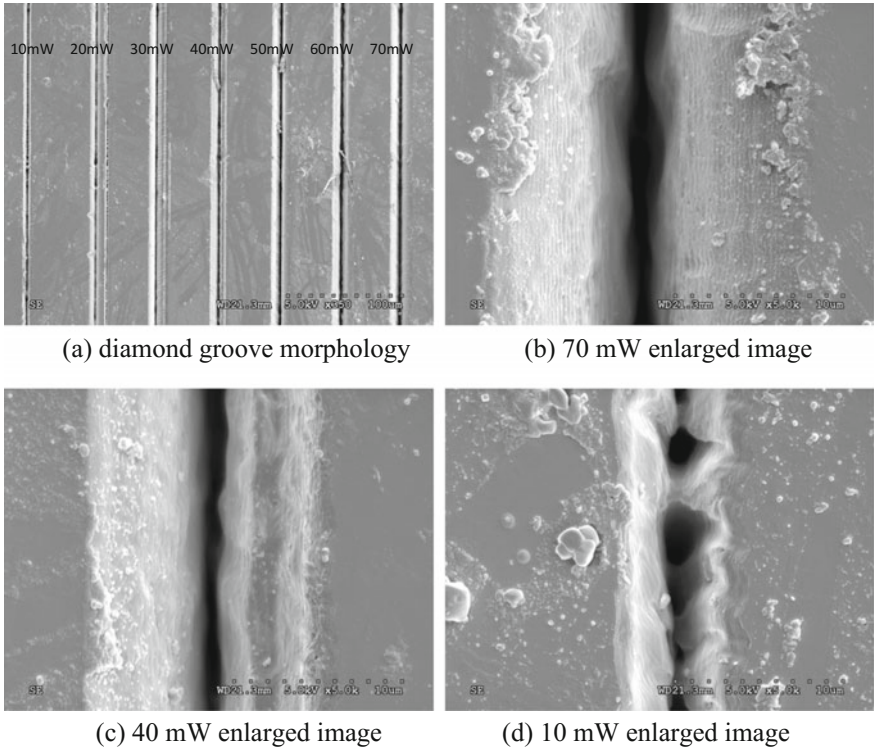(c) 40 mW enlarged image   (d) 10 mW enlarged image

Fig. 31 Effects of the laser power on diamond groove morphology

width and depth increased with a gradually decreasing rate as the laser power rising from 10 to 70 mW. Owing to Gaussian profile of the laser pulse energy, the laser fluence gradually reduces with increasing the distance to the laser spot center. The laser spot center owns the peak of laser fluence in the whole spot. Consequently, the ablation depth in the groove profile nonlinearly decreases as the increase of the distance from the groove centerline and achieves the maximum depth in the groove centerline. The change of the groove depth can be attributed to the well-known logarithmic dependence of the ablation depth and the laser fluence. In laser beam machining, the ablation depth would increase logarithmically depending on the laser fluence. Hence, the ablation depth fast increased with the increase of laser power. However, the ablation depth seems to reach a limit when the average laser power is larger than 40 mW. This is caused by the shielding effect of plasma in the depth groove.

Moreover, the groove width also shows a similar tendency with the groove depth. According to the laser ablation regime, material removal occurs in any position where the laser fluence exceeds the material damage threshold. Therefore, a smaller groove width would appear when the laser pulse energy is insufficient to assure the laser
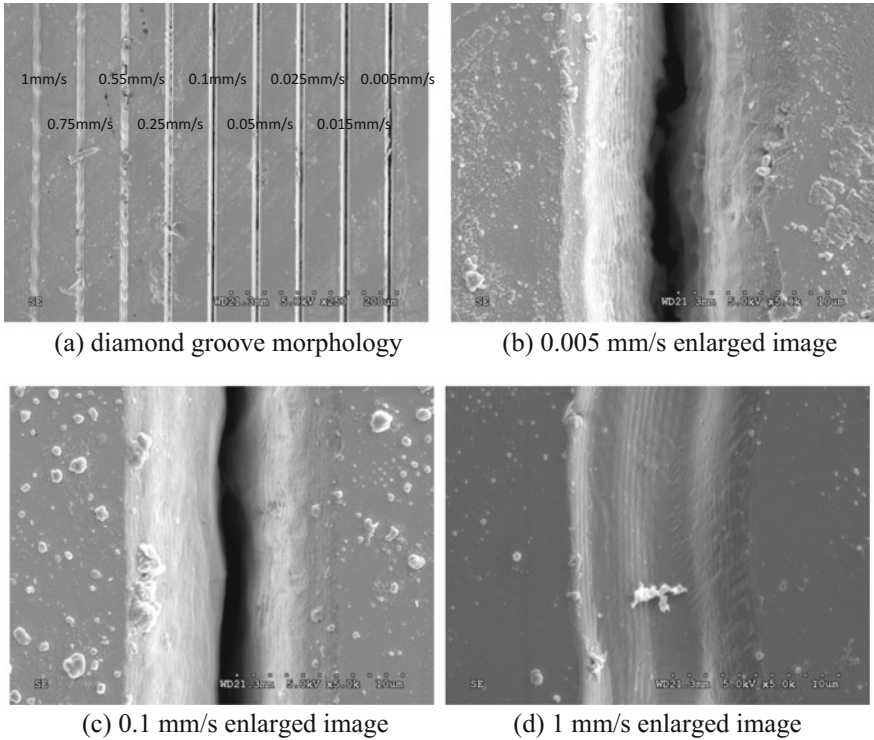
(a) diamond groove morphology

(b) 0.005 mm/s enlarged image

(c) 0.1 mm/s enlarged image

(d) 1 mm/s enlarged image

Fig. 32 Effects of the scanning speed on diamond groove morphology

fluences in the whole spot exceed the damage threshold. The reduced ablation area with lower laser power such as 10 mW induces not only a decrease of the groove width, but also a certain extent of the discontinuity at the groove bottom. As the laser power increases, the ablation width gradually tends to the spot diameter when the laser power is bigger than 40 mW and this is clearly reflected in Fig. 31. In some extent, adjusting the laser power provides us an effective method to control the groove width and depth. To obtain a larger and deeper microgroove, higher average laser power is necessary and inevitable. However, the research results also demonstrate that an excessive increase of the average laser power would result in a reduction of the energy efficiency and a further increase of the average laser power after the laser power exceeds a certain value just yields a tiny addition of the groove width or depth.

Figure 32 clearly demonstrates the influence of the scanning speed on diamond groove morphology. The groove width and depth exist a significant correlation with the scanning speed. The groove depth drops firstly with a large rate until the scanning speed reaches 0.1 mm/s and further decreases with a much lower rate as the scanning speed increased to 1.0 mm/s. In contrast, the groove width looks like keeping a stable value, while the scanning speed increases from 0.005 to 1.0 mm/s.

A further examination of the equivalent accumulated laser pulses indicates us that the increase of the scanning speed would result in a continuous reduction of the equivalent accumulated laser pulses which directly influences the total ablation depth. Moreover, the variation tendency of the accumulated laser pulses about the scanning speed is consistent with the groove depth and an obvious transition also occurs at the speed 0.1 mm/s. Therefore, the decrease of the groove depth can be attributed to the reduction of the accumulated laser pulses as the scanning speed increases. The accumulated laser pulse number just mainly influences the ablation depth, while the groove width is mainly determined by the distribution of the laser fluence. The radius where the laser fluence equals to the material damage threshold determines the ablation area and the groove width, and this radius is decided by the average laser power and independent with the accumulated laser pulses.

Based on the above experimental results, three kinds of micro-structured conditioned coarse-grained diamond grinding wheels with different abrasive grain sizes were prepared as shown in Fig. 33. The groove width of these patterns was 30 μm. The interval between two adjacent grooves was 120 μm for the parallel-line pattern. The groove direction had an angle 45° with the wheel axis direction.

The conditioned coarse-grained diamond grinding wheels were micro-structured by sub-nanosecond pulsed laser, successfully. Continuous microgroove arrays with 30 μm width were obtained on the peripheral surface of grinding wheel. The protruding parts of most diamond grits were cut-through by microgrooves. The broken diamond grit and falling off of grit were not found during laser machining.

4.2 The Effects of Micro-structured Surface on Grinding Performance

The influences of micro-structured surface on grinding performance of conditioned D213 coarse-grained diamond grinding wheels were investigated. Several optical glass BK7 workpieces were ground with the grinding wheels of abrasive grain size D91 before and after micro-structuring. The ground workpiece surface roughness Ra was measured by AFM. And the grinding force was recorded by dynamometer.

The Influence of Microstructures on Roughness
For comparatively analyzing the influence of microstructures on surface roughness, the surface roughness of single factor experiments of spindle rotation, feed rate, depth of grinding with and without microstructures are presented in Fig. 34. The surface roughness ground with non-micro-structured wheel was more insensitive to the change of the grinding parameters. Most of the roughness values were less than Ra 10 nm, while the surface roughness obtained by micro-structured wheel showed much bigger undulation. And it existed a several times increase compared to surface ground with non-micro-structured wheel. Nevertheless, grinding BK7 glass by micro-structured wheel with surface roughness less than Ra 40 nm was still feasible.
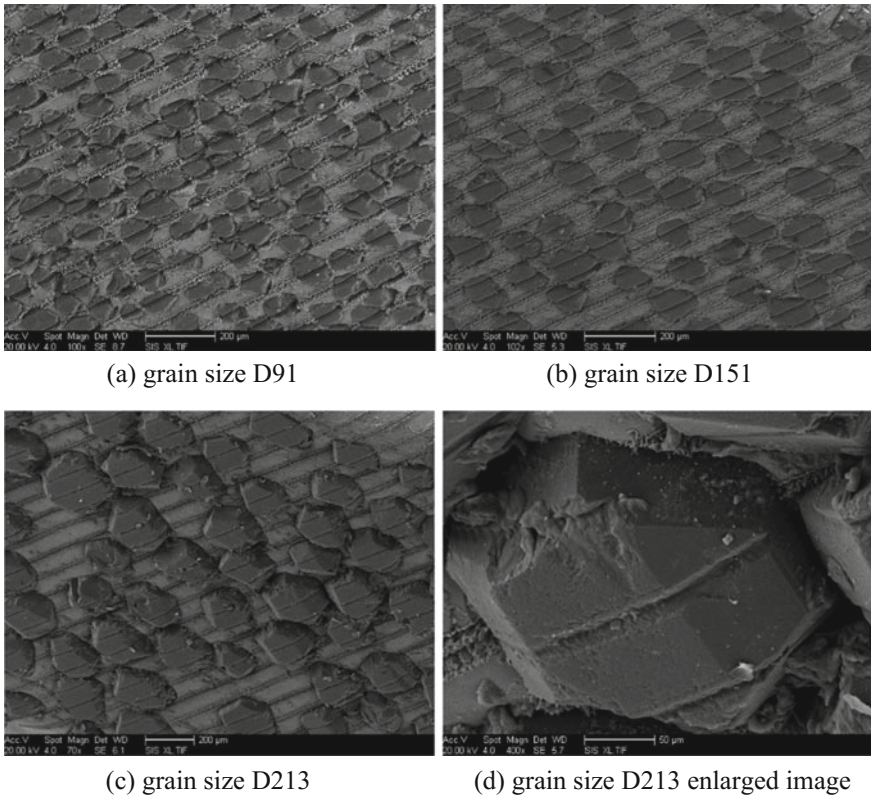
(a) grain size D91   (b) grain size D151

(c) grain size D213   (d) grain size D213 enlarged image

Fig. 33 Laser micro-structured conditioned coarse-grained diamond grinding wheels

The Influence of Microstructures on Grinding Force

As described in Fig. 35, the normal grinding force was sensitive to the change of the grinding parameters in both wheel conditions. Increasing the wheel rotation speed resulted in a gentle reduction of the normal grinding force, while the feed rate showed the opposite tendency. The normal grinding force almost linearly increased with the increase of the grinding depth in both wheel conditions. The increase of grinding depth resulted in a corresponding rise of the geometric contact length between the wheel surface and the workpiece surface. Therefore, more grain flat tops would get in contact with workpiece surface and the normal force increased.

The microstructures effectively reduced the contact area of the coarse-grained diamond tops and the workpiece surface by 33.3% thereof resulted in a decrease of the normal grinding force. Moreover, more grinding fluid could be transported into the grinding zone by the grooves, which would also be helpful for reducing the normal grinding force. The normal grinding force obtained with micro-structured wheel had a considerable reduction compared to not micro-structured wheel. Therefore, the
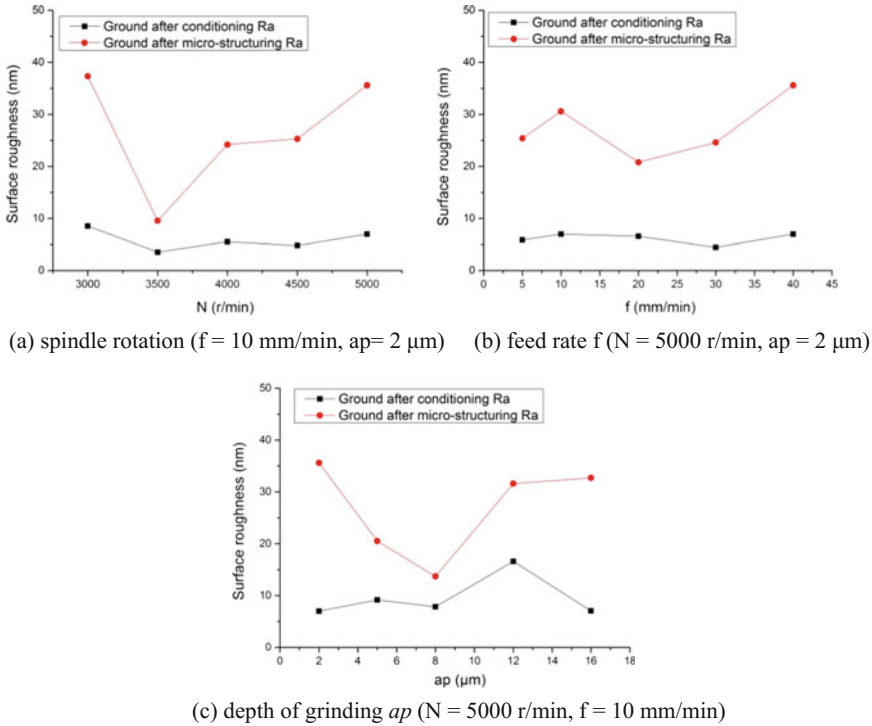
(a) spindle rotation (f = 10 mm/min, ap= 2 μm)   (b) feed rate f (N = 5000 r/min, ap = 2 μm)

(c) depth of grinding *ap* (N = 5000 r/min, f = 10 mm/min)

Fig. 34 Influence of micro-structured surface on surface roughness

normal grinding forces of grinding with surface micro-structured wheel decreased by 35–74% of grinding with surface not micro-structured wheels in the experiments.

The influence of the microstructures on tangential grinding force also shows a similar tendency with the normal grinding force, as shown in Fig. 36. The results that the tangential force of grinding operation with surface micro-structured wheel also existed a markedly decrease by 30–60% of that with non-micro-structured wheel, which proves the feasibility of using surface micro-structured wheel to reduce the grinding force once again. Furthermore, the fluctuation of the tangential grinding force of grinding operation with micro-structured wheel also decreased.

The normal-to-tangential force ratio is an important factor for analyzing the grinding process. Figure 37 shows the force ratios of grinding with wheel just conditioned and micro-structured in the order of wheel rotation, feed rate, and grinding depth. It is interesting that the force ratio almost kept consistency except in the conditions with large grinding depth. This phenomenon indicates that the grinding force of the two-wheel condition is mainly composed of the normal contact force and the friction force between the abrasive grain and workpiece surface and the force could be attributed to material removal just a small part of the total grinding force. There-
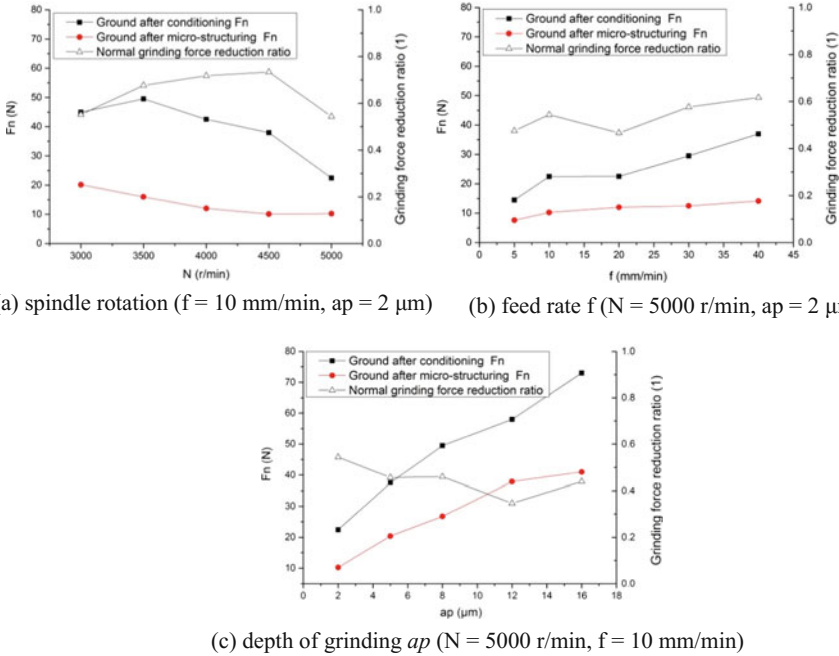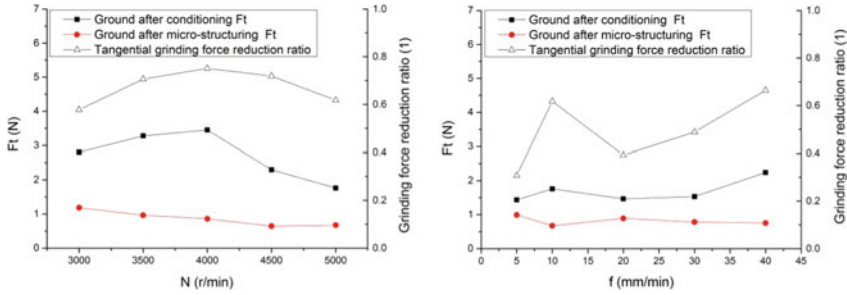
(a) spindle rotation (f = 10 mm/min, ap = 2 μm)   (b) feed rate f (N = 5000 r/min, ap = 2 μm)

(c) depth of grinding *ap* (N = 5000 r/min, f = 10 mm/min)

Fig. 35 Influence of micro-structured surface on normal grinding force

fore, micro-structuring grinding wheel surface with larger structuring ratio maybe is acceptable.
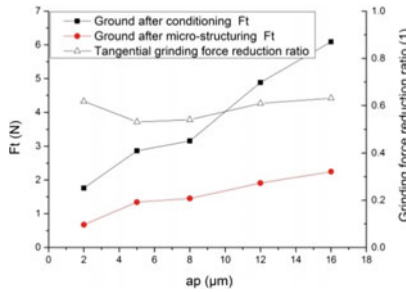
The Influence of Microstructures of Wheel Surface on Subsurface Damage

The influence of micro-structured surface on subsurface damage was investigated on BK7 glass. Four micro-structured conditioned D151 coarse-grained diamond grinding wheels with different interval microgroove arrays were machined by laser. The intervals of these grinding wheels were 30, 79, 90, and 150 μm, respectively. The grinding parameters were 3000 r/min spindle speed, 2 μm depth of grinding, and 2 mm/min feed rate. The subsurface damage was also measured by angle polishing methods. The measured results and their averaged values of subsurface crack depth are provided in Table 2.

And the SEM images of Sample 1 are shown in Fig. 38 for revealing the detail of subsurface damage. The subsurface damage depth was improved from about 10 μm (by original coarse-grained wheel, as shown in Fig. 38a) to 5 μm because of the uniform grit protrusion height due to preconditioning. The subsurface damage depth by micro-structured wheel with 150 μm interval groove arrays was further decreased to about 3 μm. Compared with the conventional coarse-grained diamond wheel, the subsurface damage depth was reduced effectually when using the micro-structured coarse-grained diamond wheel. The effect of microgroove interval on subsurface damage could be observed from Fig. 38c–f. The subsurface damage depth was
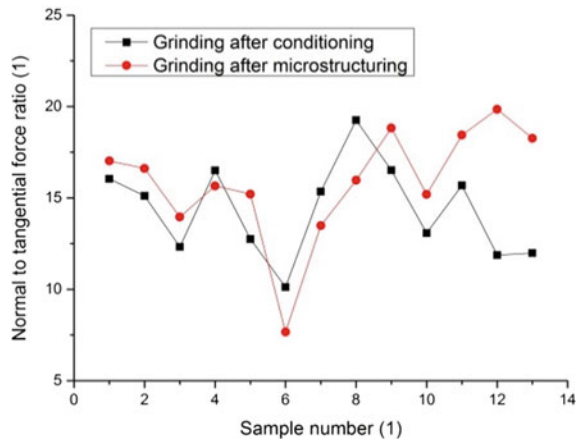
(a) spindle rotation (f = 10 mm/min, ap = 2μm)   (b) feed rate f (N = 5000 r/min, ap = 2 μm)

(c) depth of grinding *ap* (N = 5000 r/min, f = 10 mm/min)

Fig. 36 Influence of micro-structured surface on tangential grinding force

Fig. 37 Influence of micro-structured surface on normal-to-tangential force ratio

reduced with the decreasing interval. At the interval of 30 μm, the subsurface damage depth of 1.5 μm was obtained. This is mainly caused by the increase of active cutting edges and hence decreased individual chip load when using smaller interval.

It could be concluded that although grinding with micro-structured wheel induced an increase of the surface roughness, micro-structured surface was capable for effec-

Table 2 Experimental results of subsurface damage by different diamond wheels [13]

	Original wheel (µm)	Conditioned wheel without microstructures (µm)	Structured wheel (150 µm interval) (µm)	Structured wheel (90 µm interval) (µm)	Structured wheel (70 µm interval) (µm)	Structured wheel (30 µm interval) (µm)
Sample 1	7.1	5.3	2.5	2.2	2.3	1.1
Sample 2	12.5	3.4	2.5	2.1	1.7	0.9
Sample 3	11.7	6.1	3.5	2.7	2.3	1.3
Average	10.4	4.9	2.8	2.3	2.1	1.1

(a) by original wheel   (b) by conditioned wheel   (c) by 150µm interval grooves wheel

(d) by 90µm interval grooves wheel (e) by 70µm interval grooves wheel (f) by 30µm interval grooves wheel
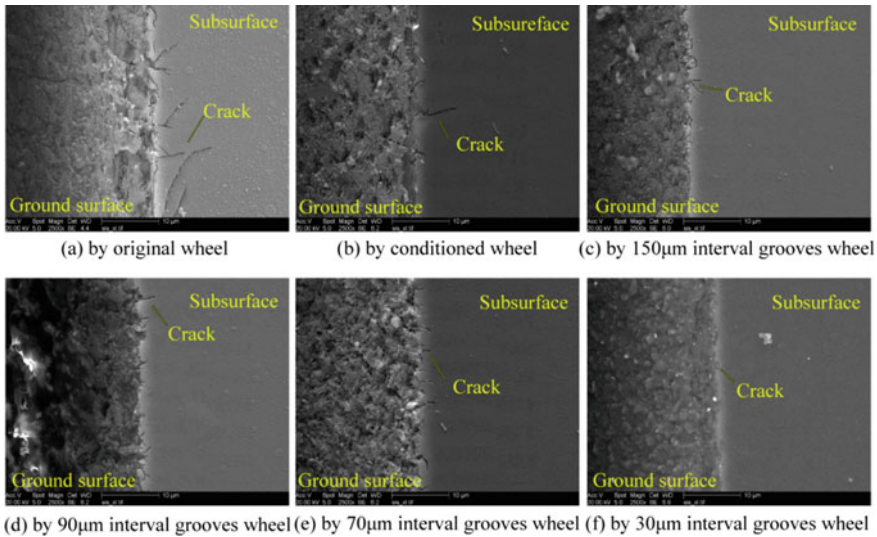
Fig. 38 SEM images of BK7 ground subsurface damage (Sample 1) [13]

tively reducing of both the normal and the tangential grinding forces for coarse-grained wheels. A reduction of 35–74% for the normal force and 30–60% for the tangential force was achieved. And thus, the subsurface damage depth reduced effectually when using the micro-structured surface on the conditioned coarse-grained diamond wheels.

5 Conclusions

In this chapter, a novel coarse-grained diamond wheel was applied which features much higher grinding ratios than that of fine-grained diamond wheels to guarantee

the machined surface form accuracy in ultra-precision grinding of hard and brittle materials.

Firstly, three kinds of conditioning technique were adopted for conditioning coarse-grained diamond wheels including ELID-assisted conditioning with metal bond diamond truer, thermochemical conditioning with metal truer, and mechanical conditioning with vitrified diamond truer. The experimental results indicated that all of three kinds of conditioning technique are applicable and feasible for conditioning coarse-grained diamond wheels, in order to realize the ultra-precision grinding of hard and brittle materials.

Secondly, the ultra-precision grinding of hard and brittle materials with coarse-grained grinding wheels was investigated. The experiments indicated the conditioned coarse-grained diamond wheels could achieve the identical surface roughness, higher form accuracy, and better wear resistance ability compared with the traditional fine-grained diamond wheels. However, deeper subsurface damage was introduced by coarse-grained diamond wheel.

Finally, for improving ground subsurface damage, the conditioned coarse-grained diamond grinding wheels were micro-structured by sub-nanosecond pulsed laser, successfully. Although the grinding process with micro-structured wheel induced an increase of the surface roughness, micro-structured surface was capable for effectively reducing of both the normal and the tangential grinding forces for coarse-grained wheels. And thus, the subsurface damage depth reduced effectually when using the micro-structured surface on the conditioned coarse-grained diamond wheels.

References

1. Brinksmeier E, Mutlugünes Y, Klocke F et al (2010) Ultra-precision grinding. CIRP Ann—-Manufact. Technol. 59(2):652–671
2. Bifano TG (1991) Ductile-regime grinding: a new technology for machining brittle materials. J Trs Asme Ser 113(2):184–189
3. Ngoi BKA, Sreejith PS (2000) Ductile regime finish machining—a review. Int J Adv Manuf Technol 16(8):547–550
4. Guo B, Zhao Q (2015) Wheel normal grinding of hard and brittle materials. Int J Adv Manuf Technol 79(5–8):873–880
5. Chen X, Rowe W B, Mills B et al (1998) Analysis and simulation of the grinding process. Part IV: Effects of wheel wear. Int J Mach Tools and Manuf 43(38):41–49
6. Zhao Q, Chen J, Yao J et al (2009) Investigation of surface and subsurface damage in diamond grinding of optical glass using hybrid copper-resin-bonded diamond wheel. J Vac Sci Technol, B 27(3):1489–1495

7. Guo B, Zhao Q (2015) Mechanical truing of V-shape diamond wheels for micro-structured surface grinding. Int J Adv Manuf Technol 78(5–8):1067–1073

8. Zhao Q, Guo B (2015) Ultra-precision grinding of optical glasses using mono-layer nickel electroplated coarse-grained diamond wheels. Part 1: ELID assisted precision conditioning of grinding wheels. Precis Eng 39:56–66

9. Ohmori H, Nakagawa T (1990) Mirror surface grinding of silicon wafers with electrolytic in-process dressing. CIRP Ann—Manuf Technol 39(1):329–332

10. Ke-Yong BI (2005) Technology of cast iron processing with diamond tool. Jewellery Sci Technol

11. Ling LZ, Zhao QL, Guo WJ et al (2013) Precision grinding of BK7 glasses using conditioned coarse-grained diamond wheel. Proc Instit Mech Eng Part B J Eng Manuf 227(10):1571–1577

12. Fateley B (1991) The handbook of IR and raman characteristic frequencies of organic molecules. Academic Press

13. Guo B, Zhao Q, Fang X (2014) Precision grinding of optical glass with laser micro-structured coarse-grained diamond wheels. J Mater Proc Tech 214(5):1045–1051

14. Guo B, Yu X, Liu X, Zhao Q et al (2018) Ultra-precision cutting of linear micro-groove array for distributed feedback laser devices. Int J Nanomanuf 14(1):9

15. Zhao Q, Guo B (2015) Ultra-precision grinding of optical glasses using mono-layer nickel electroplated coarse-grained diamond wheels. Part 2: investigation of profile and surface grinding. Precis Eng 39:67–78

16. Guo B, Wu M, Zhao Q (2017) The FEM simulation of ultra-precision grinding of optical glass with micro-structuring coarse-grained diamond wheels. Freeform Optics. JTu5A.26

17. Ling LZ, Zhao QL, Guo WJ et al (2013) Precision grinding of BK7 glasses using conditioned coarse-grained diamond wheel. Proc Inst Mech Eng Part B J Eng Manuf 227(10):1571–1577

18. Wu M, Guo B, Zhao Q et al (2018) Precision grinding of a microstructured surface on hard and brittle materials by a microstructured coarse-grained diamond grinding wheel. Ceramics Int 44(7)

19. Malkin S (1989) Grinding technology: theory and applications of machining with abrasives. SME

20. Vargas GE, Wegener K, Kuster F et al (2014) Simulation of the hone broaching process with diamond tools. J Braz Soc Mech Sci Eng 36(2):325–333

21. Bifano TG (1991) Ductile-regime grinding: a new technology for machining brittle materials. J Trs Asme Ser B 113(2):184–189

22. Heinzel C, Rickens K (2009) Engineered wheels for grinding of optical glass. CIRP Ann—Manuf Technol 58(1):315–318

23. Butler-Smith PW, Axinte DA, Pacella M et al (2013) Micro/nanometric investigations of the effects of laser ablation in the generation of micro-tools from solid CVD diamond structures. J Mater Process Technol 213(2):194–200

24. Guo B, Zhao Q, Yu X (2014) Surface micro-structuring of coarse-grained diamond wheels by nanosecond pulsed laser for improving grinding performance. Int J Precis Eng Manuf 15(10):2025–2030

25. Guo B, Wu M, Zhao Q et al (2018) Improvement of precision grinding performance of CVD diamond wheels by micro-structured surfaces. Ceram Int

26. Guo B, Zhao Q (2017) Ultrasonic vibration assisted grinding of hard and brittle linear micro-structured surfaces. Precision Eng 48:98–106